Comparison of ^{11}C-Choline and ^{18}F-FDG PET in Primary Diagnosis and Staging of Patients with Thoracic Cancer

Remge M. Pieterman, MD[1,2]; Tjin H. Que, MD[1]; Philip H. Elsinga, PhD[1]; Jan Pruim, MD[1]; John W.G. van Putten, MD[2]; Antoon T.M. Willemsen, PhD[1]; Willem Vaalburg, PhD[1]; and Harry J.M. Groen, MD[2]

[1]PET Center, Groningen University Hospital, Groningen, The Netherlands; and [2]Department of Pulmonary Diseases, Groningen University Hospital, Groningen, The Netherlands

PET with ^{18}F-FDG is used for detection and staging of thoracic cancer; however, more specific PET radiopharmaceuticals would be welcome. ^{11}C-labeled choline (CHOL) is a new radiopharmaceutical potentially useful for tumor imaging, since it is incorporated into cell membranes as phosphatidylcholine. The aim of this study was to investigate whether ^{11}C-CHOL PET has advantages over ^{18}F-FDG PET in patients with thoracic cancer. **Methods:** We evaluated 17 patients with thoracic cancer both with ^{11}C-CHOL PET and ^{18}F-FDG PET. After transmission scanning, ^{11}C-CHOL was injected intravenously, and whole-body scanning was started after 5 min. Immediately thereafter, ^{18}F-FDG was injected intravenously, followed after 90 min by interleaved attenuation-corrected whole-body scanning. Scans were performed from crown to femur. Visual and quantitative (standardized uptake value) analyses of ^{11}C-CHOL PET and ^{18}F-FDG PET were performed and compared with results of traditional staging and follow-up. **Results:** The most prominent features of normal ^{11}C-CHOL distribution were high uptake in liver, renal cortex, and salivary glands. Except for some uptake in choroid plexus and pituitary gland, brain uptake was negligible. All primary thoracic tumors were detected with ^{11}C-CHOL PET and ^{18}F-FDG PET. Both ^{11}C-CHOL PET and ^{18}F-FDG PET correctly identified all 16 patients with lymph node involvement. However, in a lesion-to-lesion analysis, ^{11}C-CHOL PET detected only 29 of 43 metastatic lymph nodes, whereas ^{18}F-FDG PET detected 41 of 43. ^{11}C-CHOL PET detected fewer intrapulmonary and pleural metastases than ^{18}F-FDG PET (27/47 vs. 46/47). More brain metastases were detected with ^{11}C-CHOL PET (23/23) than with ^{18}F-FDG PET (3/23). For primary tumors, the median (range) standard uptake values of ^{11}C-CHOL and ^{18}F-FDG were 1.68 (0.98–3.22) and 4.22 (1.40–8.26), respectively ($P = 0.001$). **Conclusion:** ^{11}C-CHOL PET can be used to visualize thoracic cancers. Although detection of lymph node metastases with ^{11}C-CHOL PET was inferior compared with ^{18}F-FDG PET, the detection of brain metastases was superior.

Key Words: ^{11}C-choline; ^{18}F-FDG; PET; thoracic cancer; metastasis

J Nucl Med 2002; 43:167–172

PET is a noninvasive metabolic imaging technique and a useful clinical tool for staging lung malignancies (*1*). Most of the experience in lung cancer imaging has been gained with the glucose analog ^{18}F-FDG, a marker of glycolysis (*2*). In the characterization of malignant solitary pulmonary nodules, ^{18}F-FDG PET yields sensitivities over 90% (*3,4*). For mediastinal staging in non–small cell lung cancer, PET is superior to CT (*1,5*). However, ^{18}F-FDG has some disadvantages; for example, uptake in inflammatory tissue may be responsible for false-positive results (*6,7*). Another problem is a reduction in cellular ^{18}F-FDG uptake in hyperglycemia (*8*). Also, routine whole-body ^{18}F-FDG PET lacks sensitivity for imaging brain metastases, a common event in lung cancer, because glucose is avidly taken up by the brain.

^{11}C-labeled choline (CHOL) has recently been described as a PET tracer for tumor detection that may not have these drawbacks (*9*). Choline is one of the components of phosphatidylcholine, an essential element of phospholipids in the cell membrane (*10*). Malignant tumors may show high proliferation and increased metabolism of cell membrane components, leading to increased uptake of choline (*11*). There is limited experience with this tracer. One study reported that it was possible to detect several different tumor types with high accuracy (*12*). Another study suggested that ^{11}C-CHOL PET was more effective than ^{18}F-FDG PET and CT in detecting very small mediastinal metastases in patients with esophageal carcinoma (*13*). Since normal brain cells are in a nondividing state, it is assumed that uptake of ^{11}C-CHOL by normal brain cells is very low. However, brain tumors and metastases are characterized by increased cell membrane synthesis, enabling them to be visualized with ^{11}C-CHOL PET (*14*). ^{11}C-CHOL is very rapidly cleared from the blood pool, and optimal tumor-to-background contrast is reached within 5 min, so scans can be started within a few minutes after injection of the radiopharmaceutical (*9,13,14*). This results in a short protocol with a minimal interval after injection of ^{11}C-CHOL, which is convenient for the patient. In contrast, ^{18}F-FDG scans are routinely started 90 minutes after injec-

Received May 1, 2001; revision accepted Oct. 24, 2001.

For correspondence or reprints contact: Harry J.M. Groen, MD, Department of Pulmonary Diseases, Groningen University Hospital, Hanzeplein 1, P.O. Box 30.001, 9700 RB Groningen, The Netherlands.

E-mail: h.j.m.groen@int.azg.nl

tion of the radiopharmaceutical to increase tumor-to-background contrast.

Considering the ability of thoracic cancers to metastasize locoregionally and hematogeneously, a whole-body PET scan to stage the disease is appealing. The aim of this study was to determine the feasibility of whole-body ^{11}C-CHOL PET for detection of primary thoracic cancers and their metastases, and to compare this technique to whole-body ^{18}F-FDG PET.

MATERIALS AND METHODS

Patients

The study population consisted of 17 patients with histologically proven thoracic cancer. Tumor size was determined by measuring the 2 largest perpendicular dimensions on a representative transverse CT slice. The minimum diameter of the primary tumor was 1 cm. Mediastinal and distant metastases were evaluated by invasive procedures such as mediastinoscopy, guided biopsy of suspected distant lesions, or subsequent imaging of growing lesions (CT, MRI, sonography, or ^{99m}Tc-diphosphonate bone scintigraphy). Patients were studied before start of treatment with chemotherapy or radiotherapy. Excluded from the study were patients with hyperglycemia before the PET study (serum glucose $\geq$10 mmol/L (180 mg/dL).

The medical ethics committee of Groningen University Hospital approved the study protocol. All patients gave written informed consent.

Data Acquisition

All studies were performed using an ECAT EXACT HR+ (Siemens/CTI Inc., Knoxville, TN). This camera acquires 63 planes simultaneously over a 15.5-cm field of view. In-plane resolution is approximately 4.3 mm, with an axial resolution of approximately 4.1 mm full width at half maximum (*15*).

^{18}F-FDG was synthesized according to Hamacher et al. (*16*) by an automated synthesis module (*17*). ^{11}C-CHOL was synthesized according to Hara et al. (*14)* by the reaction of ^{11}C-methyl iodide with dimethylaminoethanol at 100°C for 5 min. Unreacted substrates were removed by evaporation, and ^{11}C-CHOL was further purified using a cation-exchange resin. The resulting product was dissolved in saline. Both radiopharmaceuticals were sterile and their radiochemical purity was $\geq$95%.

Patients were instructed to fast for at least 6 h before imaging to minimize nonspecific uptake of ^{18}F-FDG and ^{11}C-CHOL in normal tissue (*9,18*). They were also instructed to drink at least 1 liter of water before imaging to stimulate ^{18}F-FDG excretion from the renal calyces and subsequent voiding. A venous canula was inserted in the forearm for injection of the radiopharmaceuticals. From this canula, a 2-mL blood sample was also drawn to measure serum glucose level.

After positioning the patient in the camera, transmission scanning using a ^{68}Ge/^{68}Ga ring source was performed from crown to femur for 3 min per bed position to correct for attenuation of the photons by the body tissues. This was immediately followed by intravenous injection of 800 MBq ^{11}C-CHOL. After a 5-min interval, whole-body scanning was performed over the same area for 5 min per bed position. ^{18}F-FDG was injected intravenously immediately thereafter (400 MBq in patients with body weight $<$85 kg; 600 MBq in patients with body weight $>$85 kg). Ninety minutes after ^{18}F-FDG injection (130 min after ^{11}C-CHOL administration), interleaved attenuation-corrected whole-body scanning was performed from crown to femur with 3 and 5 min per bed position for transmission and emission scanning, respectively. Data from multiple bed positions were iteratively reconstructed (ordered subset expectation maximization) into attenuated and nonattenuated ^{11}C-CHOL and ^{18}F-FDG whole-body PET images (*19*).

Data Analysis

Non–attenuation-corrected ^{11}C-CHOL PET and ^{18}F-FDG PET images were qualitatively compared for their uptake in malignant lesions and normal anatomical structures by 2 experienced PET physicians unaware of patients' clinical data. If they could not reach consensus, the opinion of a third independent observer was sought. Because detection or exclusion of malignant lesions rather than determination of quantitative parameters was the main goal of this PET study, only non–attenuation-corrected PET images were used for qualitative analysis. The physicians interpreted any hot spots as either benign or malignant.

To compare the results of ^{11}C-CHOL PET, ^{18}F-FDG PET, and histological data, mediastinal hot spots were located according to the Mountain and Dresler classification of regional lymph nodes (*20*). Hot spots outside the mediastinum were described according to anatomical location.

Standardized uptake value (SUV) was calculated for malignant primary lesions from regions of interest (ROI) obtained from the attenuation-corrected images. SUV provided a measure of tracer concentration in the ROI relative to its uniform distribution over the body. SUV depends, among other things, on patient habitus; to minimize this source of variability, a correction of SUV was made for lean body mass (*21*). Using ECAT/CAPP software (Siemens/CTI Inc.), SUVs were calculated in the transaxial plane in which the tumor had the highest activity. By using the isocontour tool adjusted to 70% of the peak counts in the lesion, an ROI was drawn from the part of the tumor with the highest activity in a standardized manner.

Statistical Analysis

The degree of interobserver agreement was quantified with the κ statistic. To compare ^{11}C-CHOL and ^{18}F-FDG SUVs of primary lung tumors, Wilcoxon's signed rank test was used. The correlation coefficient between ^{18}F-FDG and ^{11}C-CHOL SUVs was calculated using 1-tailed Pearson's test. A probability of $\leq$0.05 was considered statistically significant. Statistical analysis was performed with SPSS software (Statistical Product and Service Solutions Inc., Chicago, IL).

RESULTS

Patients

A total of 17 patients were included in this study; their characteristics are shown in Table 1. Tumor diameter varied between 2 and 8.5 cm. All 17 patients received 800 MBq ^{11}C-CHOL according to the protocol; 14 patients received 400 MBq ^{18}F-FDG, and the other 3 patients received 600 MBq ^{18}F-FDG.

Physiological Body Distribution of ^{11}C-CHOL

^{11}C-CHOL PET produced easily interpretable images. The most prominent physiological uptake of tracer was observed in the liver, renal cortex, and salivary glands. Less

TABLE 1
Patient Characteristics

Characteristic	No. of patients
Age (y) (median [range]), 58 (45–73)	
Sex (male/female)	13/4
Histology primary tumor	
Adenocarcinoma	5
Squamous cell carcinoma	2
Large cell carcinoma	5
Small cell lung cancer	2
Malignant mesothelioma	3
Stage of disease*	
Non–small cell lung cancer	
T1N0-1M0	2
T3-4N2M0	3
T2-4N0-3M1	7
Small cell lung cancer	
Extensive disease	2
Malignant mesothelioma	
T2N0M0	1
T3N3M0	1
T2N2M1	1

*The pathological tumor-nodes-metastasis (TNM) system of classification of the American Joint Committee on Cancer was used (*40*).

intense uniform tracer uptake was present in the lungs, spleen, skeletal muscles, and bone marrow. Variable ^{11}C-CHOL uptake was observed in the pancreatic region, and a linear uptake configuration in the abdomen was identified as small intestine. In 2 patients, mild uptake of ^{11}C-CHOL was observed in the thyroid gland. Uptake of tracer in the brain was negligible; however, mild tracer uptake was observed in the choroid plexus and pituitary gland. No uptake was observed in the mediastinum and myocardium. A clear distinction could be made between the mediastinum and the lungs. In 2 patients, accumulation of ^{11}C-CHOL in the bladder was observed.

The whole-body distribution of ^{18}F-FDG has been described previously (*22*). A similar pattern was observed in this study.

Detection of Lesions with ^{11}C-CHOL PET and ^{18}F-FDG PET

Interobserver Agreement. With respect to hot spot detection from ^{11}C-CHOL PET images, the degree of interobserver agreement (κ) was 0.93 (95% confidence interval [CI]; range, 0.87–0.99). For ^{18}F-FDG PET images, agreement was 0.96 (95% CI; range, 0.91–1.00). Visually, ^{11}C-CHOL uptake in malignant lesions often appeared remarkably less intense than that of ^{18}F-FDG.

Detection of Primary Thoracic Tumors. Both ^{11}C-CHOL PET and ^{18}F-FDG PET detected all 17 primary thoracic tumors (Table 2). In 4 patients the ^{11}C-CHOL hot spot appeared as a circular lesion with a rim of mild uptake and a central large defect. The matching ^{18}F-FDG hot spots appeared as circular lesions with intense increased uptake and central localized small defects.

Detection of Lymphatic Metastases. Ten patients were diagnosed with mediastinal lymph node metastases. In all

TABLE 2
Lesions Detected with ^{11}C-CHOL PET and ^{18}F-FDG PET Compared with Traditional Staging and Follow-Up*

	Lesions detected with						
	Traditional staging and follow-up		^{11}C-CHOL PET		^{18}F-FDG PET		
Localization	No. of patients	Lesions	No. of patients	Hot spots	No. of patients	Hot spots	Result†
Primary tumor	17	17	17	17	17	17	TP
Mediastinal lymph node	10	33	10	21	10	31	TP
			0	2‡	0	1‡	FP
Supraclavicular/axillar lymph node	6	10	6	8	6	10	TP
			1	1	1	1	FP
Intrapulmonary/pleural	7	47	7	27	7	46	TP
			1	1	1	1	FP
Skeleton	1	4	1	4	1	4	TP
			1	2	1	1	FP
Adrenal gland	1	1	0	0	1	1	TP
			1	1	1	1	FP
Liver	1	2	0	0	1	2	TP
Brain	3	23	3	23	2	3	TP

*Includes history, physical examination, laboratory tests, chest radiography, CT of thorax (including liver and adrenal glands), bronchoscopy with biopsy, mediastinoscopy, and, if applicable, thoracotomy. Patients with signs of distant metastases received additional imaging tests and biopsies.

†TP = true-positive; FP = false-positive.

‡Patient had false-positive and true-positive hot spots.

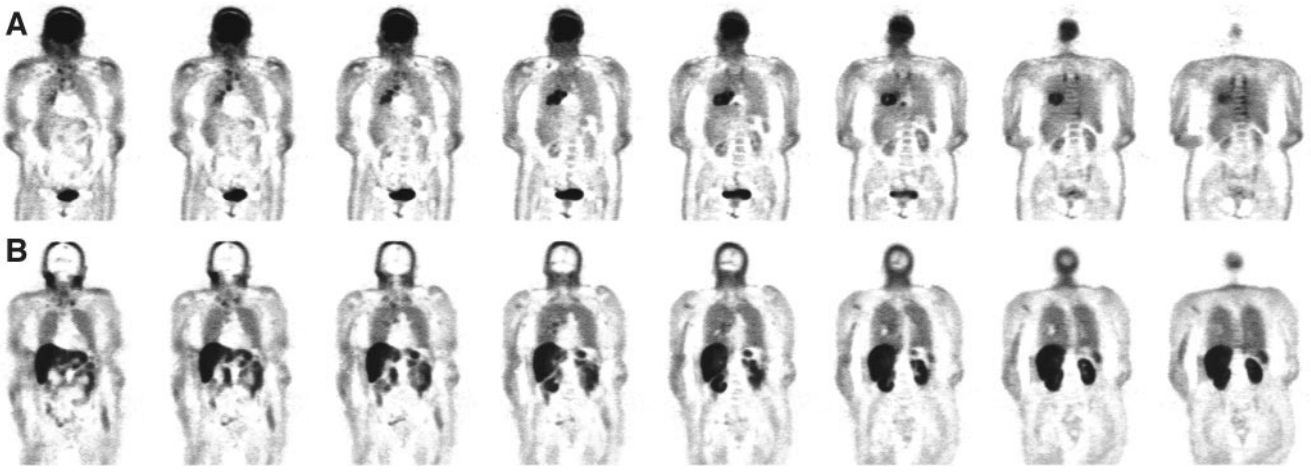

FIGURE 1. Consecutive coronal planes of non–attenuation-corrected ^{18}F-FDG PET (upper row) and ^{11}C-CHOL PET (lower row) images. ^{18}F-FDG images show intense uptake in primary tumor, hilar lymph node metastasis, and mediastinal lymph node metastases. ^{11}C-CHOL-PET images show mild tracer uptake in primary tumor and hilar metastasis; the mediastinal lymph node metastases are missed. Note high uptake of ^{11}C-CHOL-PET in liver and kidneys, hampering interpretation of upper abdomen.

these patients, both ^{11}C-CHOL PET and ^{18}F-FDG PET detected mediastinal hot spots (Table 2). With surgical procedures, a total of 33 metastatic mediastinal lymph node stations were confirmed; ^{18}F-FDG PET detected 31 of the 33 (94%), while ^{11}C-CHOL PET detected only 21 of 33 (64%) (Fig. 1). Both ^{11}C-CHOL PET and ^{18}F-FDG PET were false-positive at 1 mediastinal lymph node station in the same patient. At another mediastinal lymph node station, ^{11}C-CHOL PET, but not ^{18}F-FDG PET, was false-positive.

Both ^{11}C-CHOL PET and ^{18}F-FDG PET were correct in detecting all 6 patients with supraclavicular or axillar lymph node metastases. A total of 10 cytologically proven supraclavicular or axillar lymph node metastases were found, of which ^{11}C-CHOL PET detected 8 (80%) while ^{18}F-FDG PET detected all (100%). At 1 supraclavicular lymph node site, both ^{11}C-CHOL PET and ^{18}F-FDG PET were false-positive.

Detection of Hematogenic Metastases. Both ^{11}C-CHOL PET and ^{18}F-FDG PET correctly detected all 7 patients with intrapulmonary or pleural metastases (range, 1–23 metastases) (Table 2). In 1 patient, both ^{11}C-CHOL PET and ^{18}F-FDG PET were false-positive for 1 intrapulmonary hot spot. With ^{11}C-CHOL PET, hot spots were observed at 27 of 47 (57%) intrapulmonary or pleural metastatic sites; with ^{18}F-FDG PET, hot spots were observed at 46 of 47 (98%) sites.

In 1 patient, bone scintigraphy revealed 4 bone metastases; both ^{11}C-CHOL PET and ^{18}F-FDG PET detected skeletal hot spots at the same locations. In a second patient, ^{11}C-CHOL PET revealed hot spots in the right humerus and right pelvic bone, while ^{18}F-FDG PET only revealed a hot spot in the right humerus. Bone scintigraphy revealed no suspicious skeletal lesions at all.

An adrenal gland metastasis in 1 patient and 2 liver metastases in another patient were confirmed; these were correctly diagnosed by ^{18}F-FDG PET but not detected by ^{11}C-CHOL PET. In 1 patient, both ^{11}C-CHOL PET and ^{18}F-FDG PET were false-positive for a hot spot ranked as an adrenal gland metastasis.

CT or MRI detected 23 brain metastases in 3 patients. ^{11}C-CHOL PET was able to detect all brain metastases (100%), whereas ^{18}F-FDG PET only detected 3 (13%).

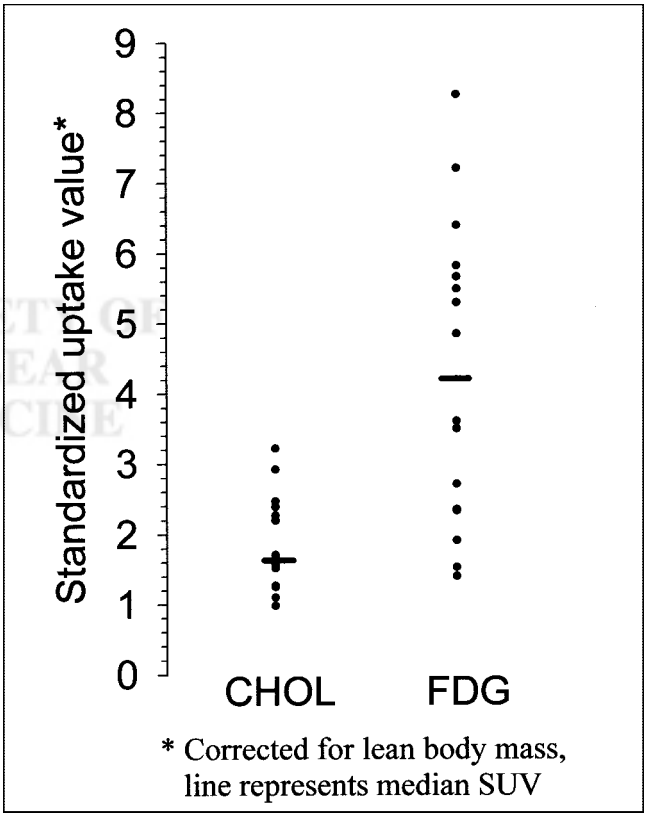

FIGURE 2. PET SUVs of ^{11}C-CHOL and ^{18}F-FDG of primary tumors in patients with thoracic cancer.

SUV Analysis

SUVs (corrected for lean body mass) of the primary lung tumor are presented in Figure 2. Apart from 1 patient, SUVs were higher for ^{18}F-FDG than for ^{11}C-CHOL. The median (range) of SUVs were 1.68 (0.98–3.22) for ^{11}C-CHOL and 4.22 (1.40–8.26) for ^{18}F-FDG ($P = 0.001$). The ^{11}C-CHOL SUV and ^{18}F-FDG SUV of primary tumors were only weakly correlated (correlation coefficient, 0.47; $P = 0.03$).

DISCUSSION

The most widely applied PET radiopharmaceutical in oncology is ^{18}F-FDG. Although ^{18}F-FDG PET studies have additional value in detection, staging, and treatment monitoring in a variety of neoplasms (*23*), ^{18}F-FDG PET is not 100% accurate in the detection of primary tumors and their metastases (*24*). Therefore, more specific PET radiopharmaceuticals are needed.

Choline is transported into cells and acts as a precursor for the biosynthesis of phospholipids, which are membrane elements (*10*). Cancer is associated with cell proliferation and upregulation of the enzyme choline kinase (which catalyzes the phosphorylation of choline in the pathway for biosynthesis of phospholipids) (*25*), providing the rationale for the use of ^{11}C-CHOL as a radiopharmaceutical in oncological PET studies. In the brain and prostate, organs in which ^{18}F-FDG PET lacks sensitivity, ^{11}C-CHOL PET showed considerable potential for the detection and staging of tumors (*14*,*26*).

PET tumor detection depends on the tumor-to-nontumor uptake ratio. Although background uptake of ^{11}C-CHOL and ^{18}F-FDG in the lung was uniform, ^{11}C-CHOL uptake in malignant lesions was lower compared with ^{18}F-FDG. The uptake of ^{11}C-CHOL in tumors represents membrane synthesis, whereas ^{18}F-FDG uptake represents glycolysis. However, ^{18}F-FDG is also taken up by inflammatory cells such as macrophages (*6*). Large cavitating lung tumors may be associated with a rim of inflammatory cells with elevated ^{18}F-FDG uptake surrounding a necrotic tumor region. Tumor hypoxia also affects cellular tracer uptake. Tumor hypoxia increases cellular uptake of ^{18}F-FDG, while the uptake of other substrates (e.g., amino acids) is decreased (*27*). Similarly, we observed reduced uptake of ^{11}C-CHOL in tumor areas that were presumed to be hypoxic.

The occurrence of locoregional or distant metastases has a profound effect on the survival of patients with thoracic cancer. Normal tracer accumulation in various organs hampers the detection of metastases with PET in these organs. In the case of ^{11}C-CHOL, free intracellular choline is not only phosphorylated, but it can also be oxidized to betaine aldehyde (*10*). Since the liver and kidney are major sites for choline oxidation, they exhibit a high background uptake (*26*,*28*). For this reason, liver and adrenal gland metastases were not detected by ^{11}C-CHOL PET nearly as well as by ^{18}F-FDG PET. The enhanced uptake of ^{11}C-CHOL observed in the pancreas and intestine of several patients may be due to secretion of phospholipid-rich pancreatic juice and bile (*9*,*26*,*29*).

Consistent with previously reported data (*14*,*30*), ^{11}C-CHOL PET was very effective in detecting brain metastases. ^{11}C-CHOL penetrates the blood–brain barrier by the amine-specific transport system (*31*), followed by a rapid brain washout (*28*). Disruption of the blood–brain barrier is observed in brain tumors and metastases, and this may facilitate increased ^{11}C-CHOL uptake for cell membrane synthesis. Incorporation of ^{11}C-CHOL in the endothelium of cerebral blood vessels present in the choroid plexus and pituitary gland (*32*), which do not have a blood–brain barrier, may explain the increased uptake at these sites. Because of the excessive uptake of glucose in the brain, a routine whole-body ^{18}F-FDG PET lacks the sensitivity to detect brain metastases. Other ^{11}C-labeled radiopharmaceuticals used for the evaluation of brain tumors include ^{11}C-methionine and ^{11}C-tyrosine (*33*,*34*). In the detection of brain tumors, ^{11}C-CHOL may be preferred to amino acids due its higher tumor-to-background ratio (*14*). The detection of bone (marrow) metastases with ^{11}C-CHOL PET and ^{18}F-FDG PET in this study was consistent with the literature (*26*,*35*,*36*). In 2 patients ^{11}C-CHOL uptake in the urinary bladder was observed. This urinary accumulation of ^{11}C-CHOL may be the result of incomplete tubular reabsorption of intact tracer or enhanced excretion of labeled oxidative metabolites (*9*), as was also suggested by DeGrado et al. (*37*), who saw accumulation in the bladder while using ^{18}F-labeled choline.

^{11}C-CHOL PET and ^{18}F-FDG PET were equally accurate in detecting lymph node metastases. However, on a lesion-to-lesion basis, ^{11}C-CHOL PET was less sensitive than ^{18}F-FDG PET. Our observations contrast with those of Hara et al. (*38*), who observed 100% sensitivity for ^{11}C-CHOL PET and 75% sensitivity for ^{18}F-FDG PET in detecting mediastinal lymph node metastases originating from non–small cell lung cancer. This may be partly explained by the low SUV threshold used by Hara et al., as they defined a 40% difference from the SUV of the primary tumor as positive for mediastinal lymph node metastasis. This will easily lead to a high sensitivity for ^{11}C-CHOL PET. Their low sensitivity of ^{18}F-FDG PET could be explained by the short interval of 40 min between the injection of ^{18}F-FDG and the onset of scanning. Tumor concentrations of ^{18}F-FDG do not reach a plateau until 90 min after intravenous injection (*39*).

Consistent with previous reports, ^{11}C-CHOL PET gave clear images with good contrast at 5 min after injection (*26*,*35*). After intravenous injection, tissue uptake and blood clearance is rapid, and the tissue-to-background ratio remains essentially constant over 30 min (*9*,*35*). Although the short half-life of ^{11}C-labeled radiopharmaceuticals could limit the applicability of whole-body scanning, we found that PET with 800 MBq ^{11}C-CHOL was feasible in practice to obtain images from crown to femur in thoracic cancer patients. According to our acquisition protocol, the ^{18}F-FDG

scan was started 130 min after the ^{11}C-CHOL injection, which is more than 6 half-lives of ^{11}C. It can be assumed that ^{18}F-FDG scanning is not contaminated by residual ^{11}C radioactivity. Whole-body PET to stage thoracic cancer is appealing considering the ability of this disease to metastasize locoregionally and hematogeneously.

CONCLUSION

Visual analysis of whole-body ^{11}C-CHOL PET was less accurate than that of whole-body ^{18}F-FDG PET for the detection of metastases in thoracic cancer patients due to the lower accumulation of ^{11}C-CHOL in malignant tissue. The inferiority of ^{11}C-CHOL PET was most notable in the detection of lymph node metastases. However, for the detection of brain metastases, ^{11}C-CHOL PET was superior to ^{18}F-FDG PET.

REFERENCES

1. Pieterman RM, van Putten JW, Meuzelaar JJ, et al. Preoperative staging of non-small-cell lung cancer with positron-emission tomography. *N Engl J Med.* 2000;343:254–261.
2. Nolop KB, Rhodes CG, Brudin LH, et al. Glucose utilization in vivo by human pulmonary neoplasms. *Cancer.* 1987;60:2682–2689.
3. Dewan NA, Gupta NC, Redepenning LS, Phalen JJ, Frick MP. Diagnostic efficacy of PET-FDG imaging in solitary pulmonary nodules. Potential role in evaluation and management. *Chest.* 1993;104:997–1002.
4. Lowe VJ, Fletcher JW, Gobar L, et al. Prospective investigation of positron emission tomography in lung nodules. *J Clin Oncol.* 1998;16:1075–1084.
5. Vansteenkiste JF, Stroobants SG, De Leyn PR, et al. Lymph node staging in non-small-cell lung cancer with FDG-PET scan: a prospective study on 690 lymph node stations from 68 patients. *J Clin Oncol.* 1998;16:2142–2149.
6. Kubota R, Yamada S, Kubota K, et al. Intratumoral distribution of fluorine-18-fluorodeoxyglucose in vivo: high accumulation in macrophages and granulation tissues studied by microautoradiography. *J Nucl Med.* 1992;33:1972–1980.
7. Lewis PJ, Salama A. Uptake of fluorine-18-fluorodeoxyglucose in sarcoidosis. *J Nucl Med.* 1994;35:1647–1649.
8. Langen KJ, Braun U, Rota KE, et al. The influence of plasma glucose levels on fluorine-18- fluorodeoxyglucose uptake in bronchial carcinomas. *J Nucl Med.* 1993;34:355–359.
9. Roivainen A, Forsback S, Grönroos T, et al. Blood metabolism of (methyl-^{11}C)choline; implications for in vivo imaging with positron emission tomography. *Eur J Nucl Med.* 2000;27:25–32.
10. Zeisel SH. Dietary choline: biochemistry, physiology, and pharmacology. *Annu Rev Nutr.* 1981;1:95–121.
11. Podo F. Tumour phospholipid metabolism. *NMR Biomed.* 1999;12:413–439.
12. Hara T, Kosaka N, Kondo T, Kishi H, Kobori O. Imaging of brain tumor, lung cancer, esophagus cancer, colon cancer, prostate cancer, and bladder cancer with (C-11)choline [abstract]. *J Nucl Med.* 1997;38(suppl):250P.
13. Kobori O, Kirihara Y, Kosaka N, Hara T. Positron emission tomography of esophageal carcinoma using (11)C- choline and (18)F-fluorodeoxyglucose: a novel method of preoperative lymph node staging. *Cancer.* 1999;86:1638–1648.
14. Hara T, Kosaka N, Shinoura N, Kondo T. PET imaging of brain tumor with [methyl-11C]choline. *J Nucl Med.* 1997;38:842–847.
15. Brix G, Zaers J, Adam LE, et al. Performance evaluation of a whole-body PET scanner using the NEMA protocol. *J Nucl Med.* 1997;38:1614–1623.
16. Hamacher K, Coenen HH, Stocklin G. Efficient stereospecific synthesis of no-carrier-added 2-[18F]-fluoro-2- deoxy-D-glucose using aminopolyether supported nucleophilic substitution. *J Nucl Med.* 1986;27:235–238.
17. Medema J, Luurtsema G, Keizer H, et al. Performance of a fully automated and unattended production system of (^{18}F)FDG [abstract]. *J Labelled Compd Radiopharm.* 1999;42(suppl):s853-s855.
18. Schelbert HR, Hoh CK, Royal HD, et al. Procedure guideline for tumor imaging using fluorine-18-FDG. *J Nucl Med.* 1998;39:1302–1305.
19. Lonneux M, Borbath I, Bol A, et al. Attenuation correction in whole-body FDG oncological studies: the role of statistical reconstruction. *Eur J Nucl Med.* 1999;26:591–598.
20. Mountain CF, Dresler CM. Regional lymph node classification for lung cancer staging. *Chest.* 1997;111:1718–1723.
21. Zasadny KR, Wahl RL. Standardized uptake values of normal tissues at PET with 2-[fluorine- 18]-fluoro-2-deoxy-D-glucose: variations with body weight and a method for correction. *Radiology.* 1993;189:847–850.
22. Cook GJ, Fogelman I, Maisey MN. Normal physiological and benign pathological variants of 18-fluoro-2- deoxyglucose positron-emission tomography scanning: potential for error in interpretation. *Semin Nucl Med.* 1996;26:308–314.
23. Hoh CK, Schiepers C, Seltzer MA, et al. PET in oncology: will it replace the other modalities? *Semin Nucl Med.* 1997;27:94–106.
24. Strauss LG. Fluorine-18 deoxyglucose and false-positive results: a major problem in the diagnostics of oncological patients. *Eur J Nucl Med.* 1996;23:1409–1415.
25. Katz-Brull R, Degani H. Kinetics of choline transport and phosphorylation in human breast cancer cells; NMR application of the zero trans method. *Anticancer Res.* 1996;16:1375–1380.
26. Hara T, Kosaka N, Kishi H. PET imaging of prostate cancer using carbon-11-choline. *J Nucl Med.* 1998;39:990–995.
27. Clavo AC, Wahl RL. Effects of hypoxia on the uptake of tritiated thymidine, L-leucine, L- methionine and FDG in cultured cancer cells. *J Nucl Med.* 1996; 37:502–506.
28. Friedland RP, Mathis CA, Budinger TF, Moyer BR, Rosen M. Labeled choline and phosphorylcholine: body distribution and brain autoradiography [concise communication]. *J Nucl Med.* 1983;24:812–815.
29. Hay DW, Carey MC. Chemical species of lipids in bile. *Hepatology.* 1990; 12(suppl):6S-14S.
30. Shinoura N, Nishijima M, Hara T, et al. Brain tumors: detection with C-11 choline PET. *Radiology.* 1997;202:497–503.
31. Pardridge WM. Transport of nutrients and hormones through the blood-brain barrier. *Fed Proc.* 1984;43:201–204.
32. Estrada C, Bready J, Berliner J, Cancilla PA. Choline uptake by cerebral capillary endothelial cells in culture. *J Neurochem.* 1990;54:1467–1473.
33. Ogawa T, Shishido F, Kanno I, et al. Cerebral glioma: evaluation with methionine PET. *Radiology.* 1993;186:45–53.
34. Pruim J, Willemsen AT, Molenaar WM, et al. Brain tumors: L-[1-C-11]tyrosine PET for visualization and quantification of protein synthesis rate. *Radiology.* 1995;197:221–226.
35. Kotzerke J, Prang J, Neumaier B, et al. Experience with carbon-11 choline positron emission tomography in prostate carcinoma. *Eur J Nucl Med.* 2000;27: 1415–1419.
36. Bury T, Barreto A, Daenen F, et al. Fluorine-18 deoxyglucose positron emission tomography for the detection of bone metastases in patients with non-small cell lung cancer. *Eur J Nucl Med.* 1998;25:1244–1247.
37. DeGrado TR, Coleman RE, Wang S, et al. Synthesis and evaluation of 18F-labeled choline as an oncologic tracer for positron emission tomography: initial findings in prostate cancer. *Cancer Res.* 2001;61:110–117.
38. Hara T, Inagaki K, Kosaka N, Morita T. Sensitive detection of mediastinal lymph node metastasis of lung cancer with 11C-choline PET. *J Nucl Med.* 2000;41: 1507–1513.
39. Hamberg LM, Hunter GJ, Alpert NM, et al. The dose uptake ratio as an index of glucose metabolism: useful parameter or oversimplification? *J Nucl Med.* 1994; 35:1308–1312.
40. Mountain CF. Revisions in the International System for Staging Lung Cancer. *Chest.* 1997;111:1710–1717.